# $^{89}$Zr-Chloride Can Be Used for Immuno-PET Radiochemistry Without Loss of Antigen Reactivity In Vivo

Darpan N. Pandya[1], Nikunj B. Bhatt[1], Frankis Almaguel[2], Stephanie Rideout-Danner[2], Howard D. Gage[2], Kiran Kumar Solingapuram Sai[2], and Thaddeus J. Wadas[1]

*[1]Department of Cancer Biology, Wake Forest University Health Sciences, Winston-Salem, North Carolina; and [2]Department of Radiology, Wake Forest University Health Sciences, Winston-Salem, North Carolina*

$^{89}$Zr immuno-PET continues to be assessed in numerous clinical trials. This report evaluates the use of $^{89}$Zr-chloride in the radiolabeling of monoclonal antibodies conjugated with desferrioxamine B (DFO), describes its effects on radiopharmaceutical reactivity toward antigen, and offers guidance on how to ensure long-term stability and purity. **Methods:** $^{89}$Zr-DFO-trastuzumab and $^{89}$Zr-DFO-cetuximab were prepared using $^{89}ZrCl_4$. The stability of each was evaluated for 7 d in 20 mM histidine/240 mM sucrose buffer, 0.25 M sodium acetate (NaOAc) buffer containing 5 mg·mL$^{-1}$ *n*-acetyl-L-cysteine (NAC), or 0.25 M NaOAc containing 5 mg·mL$^{-1}$ L-methionine (L-MET). To assess antigen reactivity, $^{89}$Zr-DFO-trastuzumab was evaluated using the Lindmo method and tested in PET/CT imaging of mouse models of human epidermal growth factor receptor 2–positive or –negative lung cancer. **Results:** Using $^{89}ZrCl_4$, $^{89}$Zr-DFO-trastuzumab and $^{89}$Zr-DFO-cetuximab were prepared with increased specific activity and retained purities of 95% after 3 d when formulated in NaOAc buffer containing L-MET. Based on Lindmo analysis and small-animal PET/CT imaging, $^{89}$Zr-DFO-trastuzumab remained reactive toward antigen after being prepared with $^{89}ZrCl_4$. **Conclusion:** $^{89}ZrCl_4$ facilitated the radiosynthesis of $^{89}$Zr immuno-PET agents with increased specific activity. L-MET enhanced long-term solution stability better than all other formulations examined, and $^{89}$Zr-DFO-trastuzumab remained reactive toward antigen. Although further evaluation is necessary, these initial results suggest that $^{89}ZrCl_4$ may be useful in immuno-PET radiochemistry as radiolabeled monoclonal antibodies are increasingly integrated into precision medicine strategies.

**Key Words:** $^{89}$Zr chloride; stability; immuno-PET

**J Nucl Med 2019; 60:696–701**
DOI: 10.2967/jnumed.118.216457

Precision medicine describes a clinical care strategy that creates a treatment plan based on the genetic and phenotypic characteristics of a patient's underlying disease (*1*). In oncology, this approach has relied on targeting molecular pathways and activating the immune system to eliminate cancerous cells. However, to be truly efficient, precision medicine strategies require the codevelopment of diagnostic technologies that enable providers to select treatments with the maximum clinical benefit (*2*). For example, cetuximab and trastuzumab are therapeutic monoclonal antibodies (mAbs) that target the epidermal growth factor receptor (EGFR) and human epidermal growth factor receptor 2 (HER2), respectively; these receptors are overexpressed by a variety of cancers (*3*). Radiolabeled PET analogs, which have been used to detect disease, perform patient stratification, and monitor therapeutic response, are facilitating the successful integration of these mAbs into precision medicine strategies (*4*).

$^{89}$Zr (half-life, 78.4 h; $\beta^+$, 22.8%; $E_{\beta+max}$, 901 keV; electron capture, 77%; $E_\gamma$, 909 keV; 99%) is currently being used to radiolabel mAbs, since its nuclear decay and the biologic half-life of a circulating mAb are complementary (*4*). The current strategy to prepare clinical $^{89}$Zr-radiopharmaceuticals relies on the reaction of $^{89}$Zr-oxalate ($^{89}Zr(ox)_2$) with the bifunctional chelator derivatives of desferrioxamine B (DFO) (*5*). However, the use of $^{89}Zr(ox)_2$ as a starting material has always been viewed as problematic (*6,7*). Although replacing it with $^{89}$Zr-chloride ($^{89}ZrCl_4$) has been suggested, the perceived radiolysis-induced degradation that a mAb may experience in the presence of ionizing radiation and aqueous chloride anions lessened enthusiasm for this approach. However, its recent use in the preparation of $^{89}$Zr-tetraazamacrocycle complexes has renewed interest in the application of this $^{89}$Zr source to $^{89}$Zr immuno-PET agent synthesis (*8–10*). Here we describe our initial studies to investigate the use of $^{89}ZrCl_4$ in $^{89}$Zr-radiopharmaceutical development.

## MATERIALS AND METHODS

$^{89}Zr(ox)_2$ was purchased from Sophie, Inc., and converted to $^{89}ZrCl_4$ (Supplemental Fig. 1; supplemental materials are available at http://jnm.snmjournals.org) using a modified procedure (*8*). Briefly, an $^{89}Zr(ox)_2$ (1,810–1,890 MBq) solution in 1.0 M oxalic acid was loaded onto an activated Waters Sep-Pak Light Accell Plus QMA strong anion exchange cartridge (300 Å pore size, 37- to 55-μm particle size, 230 μeq/g ion exchange capacity), prewashed with 6 mL of MeCN, 10 mL of 0.9% saline, and 10 mL of water. The cartridge was then washed with water (>50 mL) to remove oxalic acid and the activity eluted with a 99% recovery of $^{89}$Zr by chloride ion exchange with 400–500 μL of 1.0 M HCl (aqueous).

Chemicals were purchased from Sigma-Aldrich Chemical Co., and solutions were prepared with ultrapure water (18 MΩ-cm resistivity). *p*-isothiocyanatobenzyl-desferrioxamine was purchased from Macrocyclics, Inc. Trastuzumab and cetuximab were acquired from Myoderm, Inc. Female athymic *nu/nu* mice (6 wk) were purchased from Jackson Laboratories, and NCI-H2170 (HER2-positive [HER2$^+$]) cells or HCC-827 (HER2-negative [HER2$^-$]) cells were obtained from ATCC.

Received Jul. 20, 2018; revision accepted Oct. 2, 2018.
For correspondence or reprints contact: Thaddeus J. Wadas, Department of Cancer Biology, Wake Forest University Health Sciences, One Medical Center Blvd., Winston-Salem, NC 27157.
E-mail:twadas@wakehealth.edu
Published online Nov. 15, 2018.

**TABLE 1**
Comparison of $^{89}Zr(ox)_2$ and $^{89}ZrCl_4$ Used to Prepare $^{89}Zr$ Immuno-PET Agents

| Parameter | $^{89}Zr(ox)_2$ | | | $^{89}ZrCl_4$ in this work |
|---|---|---|---|---|
| | Perk et al.* | Knight et al.† | This work | |
| mAb (mg)‡ | 0.7–3.0 | 0.1 | 0.35 | 0.25 |
| $^{89}Zr$ added (MBq) | 37–250 | 10 | 40–45 | 40–45 |
| Oxalic acid neutralization method | 2 M $Na_2CO_3$ | 1 M $Na_2CO_3$ | 2 M $Na_2CO_3$ | None |
| Reaction buffer | 0.5 M HEPES¶ | PBS§ | 0.5 M HEPES¶ | 0.5 M HEPES¶ |
| Final reaction pH | 6.8–7.2 | 7–8 | 6.8–7.2 | 6.8–7.2 |
| Reaction temperature (°C) | 21–24 | 21–24 | 21–24 | 21–24 |
| Reaction time (h) | 1 | 1 | 1 | 0.25 |
| Radiolabeling yield (%) | >80 | 96.9 ± 3.3 | ≥95‖ | ≥97.5‖ |
| Radiochemical purity (%) | >95 | >95 | ≥96‖ | ≥97.5‖ |
| Specific activity (MBq $\mu g^{-1}$) | 0.067–0.086 | 0.1 ± 0.03 | 0.105 ± 0.003 ($n$ = 10)# | 0.174 ± 0.003 ($n$ = 10)# |

*Adapted from (*15*).
†Adapted from (*18*).
‡Mass mAb used in radiochemical synthesis.
¶pH 7.1–7.3.
§pH 7.4.
‖Unchelated $^{89}Zr$ was not present in original reaction mixture as determined by Radio–instant thin-layer chromatography. Final purity and yield reflect presence of high- and low-molecular-weight species, which were additionally determined by size-exclusion chromatography.
#$^{89}Zr$-DFO-trastuzumab ($n$ = 5) and $^{89}Zr$-DFO-cetuximab ($n$ = 5).
PBS = phosphate-buffered saline.

Radiochemistry reaction progress and purity were monitored using size-exclusion chromatography and radio–thin-layer chromatography analysis, whereas the amount of radioactivity in each sample was assessed using a radioisotope calibrator or γ-counter as previously described (*11*). PET and CT images were acquired using a TriFoil small-animal PET/CT scanner.

The preparation of DFO-mAbs, the determination of chelator-to-mAb ratio (Supplemental Table 1), and the preparation of $^{89}Zr$-DFO-mAbs using $^{89}Zr(ox)_2$ (Supplemental Table 2) were accomplished as previously described (*11*). For DFO-mAb radiochemistry involving $^{89}ZrCl_4$ (Supplemental Scheme 1), $^{89}ZrCl_4$ (40–45 MBq in 20–25 μL of 1.0 M HCl) was placed in a 1.5-mL tube. The pH was adjusted to 6.8–7.2 using 0.5 M (4-(2-hydroxyethyl)-1-piperazineethanesulfonic acid) (HEPES) buffer (500 μL, pH 7.2). Next, sodium acetate buffer (NaOAc; 200 μL, 0.25 M, pH 6.8–7.0) containing L-methionine (L-MET; 5 $mg \cdot mL^{-1}$) and 250 μg of DFO-mAb conjugate (83 μL saline) were added followed by a 15-min incubation period at 21°C. The crude reaction mixture was purified using a PD-10 column and 0.25 M NaOAc/L-MET (5 mg $mL^{-1}$; pH 6.8–7.0) as eluent. $^{89}Zr$-DFO-mAbs, which were prepared using $^{89}ZrCl_4$ and formulated in 0.25 M NaOAc buffer containing *n*-acetyl-L-cysteine (NAC; 5 $mg \cdot mL^{-1}$; pH 6.8–7.0) or 20 mM histidine/240 mM sucrose, was accomplished using previously published procedures (*11*). Radiochemical yield and purity of $^{89}Zr$-DFO-mAbs were determined as previously described (*11*). For in vitro stability studies, $^{89}Zr$-DFO-trastuzumab and $^{89}Zr$-DFO-cetuximab (both 9.3 MBq) were formulated in different buffer-excipient combinations and analyzed for 7 d as previously described (*11*).

To describe the interaction of $^{89}Zr$-DFO-trastuzumab with the HER2 receptor, the immunoreactivity (IR), association constant ($K_a$), and number of binding sites per cell ($B_{max}$) were determined using the Lindmo method and Scatchard analysis (*12,13*).

Animal studies were performed under a protocol approved by the Wake Forest University Health Sciences Institutional Animal Care and Use Committee. Mice were inoculated with $1 \times 10^7$ cells in contralateral flanks, and tumor growth was evaluated as described previously (*11*). Tumor-bearing mice ($n$ = 5/group) received an injection of $^{89}Zr$-DFO-trastuzumab (8.9–10.2 MBq in 150 μL/mouse) via the tail vein and were imaged at 24, 72, and 144 h after injection. Images were reconstructed and coregistered with CT, and the percentage injected dose of activity per gram of tissue was determined at every time point using a known procedure (*8*). At 144 h, a post-PET biodistribution study was performed, and the percentage injected dose per gram of tissue was determined using a known procedure (*8*).

All plots were generated using GraphPad Prism 5.0 software. All data are presented as mean with either SD or 95% confidence interval. Student $t$ tests (2-tailed, unpaired) or 1-way ANOVA with Tukey multiple comparison posttests were performed. A $P$ value of less than 0.05 was considered statistically significant.

## RESULTS

$^{89}ZrCl_4$ was prepared using a modified method (*8*). Typically, 1,850 MBq of $^{89}Zr(ox)_2$ was loaded on the ion exchange cartridge and eluted as $^{89}ZrCl_4$ in 500 μL of 1 M HCl with a 99% recovery yield. In our hands, the conversion process took 10 min to complete and the resulting $^{89}ZrCl_4$ was used to prepare $^{89}Zr$-DFO-trastuzumab and $^{89}Zr$-DFO-cetuximab without further manipulation. The results of radiochemistry studies are summarized in Table 1 and Supplemental Tables 2 and 3. Using $^{89}ZrCl_4$, we prepared both radiopharmaceuticals in 15 min, with radiochemical purities and yields greater than 97% (Supplemental Figs. 2 and 3).

The in vitro stability of $^{89}$Zr-DFO-trastuzumab and $^{89}$Zr-DFO-cetuximab was examined using centrifugal filtration analysis with γ-counting (Supplemental Tables 4 and 5), radio–instant thin-layer chromatography (Supplemental Figs. 4 and 5; Supplemental Tables 6 and 7), and radio–size-exclusion chromatography (Fig. 1; Supplemental Figs. 6–8; Supplemental Tables 8 and 9) after being prepared with $^{89}ZrCl_4$, and formulated in 20 mM histidine/240 mM sucrose buffer, 0.25 M NaOAc buffer containing 5 mg·mL$^{-1}$ NAC, or 0.25 M NaOAc containing 5 mg·mL$^{-1}$ L-MET. When formulated in 20 mM histidine/240 mM sucrose buffer and stored at 21°C, both radiopharmaceuticals remained stable for 6 h, with radiochemical impurities comprising less than 5% of the total reaction mixture. By 1 d, however, purity decreased to 90%, and it continued to decrease throughout the study. When both radiopharmaceuticals were formulated in 0.25 M NaOAc buffer containing 5 mg·mL$^{-1}$ NAC and stored at 21°C, radiopharmaceutical purity remained above 95% for 24 h, but declined to 80% by the end of the study. When $^{89}$Zr-DFO-trastuzumab was formulated in 0.25 M NaOAc containing 5 mg·mL$^{-1}$ L-MET and stored at 21°C, radiopharmaceutical purity, as assessed by radio–size-exclusion chromatography, remained above 95% for 3 d (average percentage intact at 3 d for 20 mM histidine/240 mM sucrose vs. 0.25 M NaOAc/5 mg·mL$^{-1}$ NAC vs. 0.25 M NaOAc/5 mg·mL$^{-1}$ L-MET: 74.9 ± 0.4 vs. 85.3 ± 0.2 vs. 95.5 ± 0.1; 1-way ANOVA: $F_{3208,0.99} = 635.1$, $P < 0.0001$). This result was recapitulated with $^{89}$Zr-DFO-cetuximab (average percentage intact at 3 d for 20 mM histidine/240 mM sucrose vs. 0.25 M NaOAc/5 mg·mL$^{-1}$ NAC vs. 0.25 M NaOAc/5 mg·mL$^{-1}$ L-MET: 64.1 ± 0.5 vs. 88.7 ± 0.1 vs. 95.1 ± 0.1; 1-way ANOVA: $F_{9914,0.999} = 1{,}609$, $P < 0.0001$). Finally, both radiopharmaceuticals, which were initially formulated in 0.25 M NaOAc containing 5 mg·mL$^{-1}$ L-MET, were stable in human serum over 7 d. Serum-associated radioactivity comprised less than 5% of the total reaction mixture at the end of the study (Supplemental Table 10).

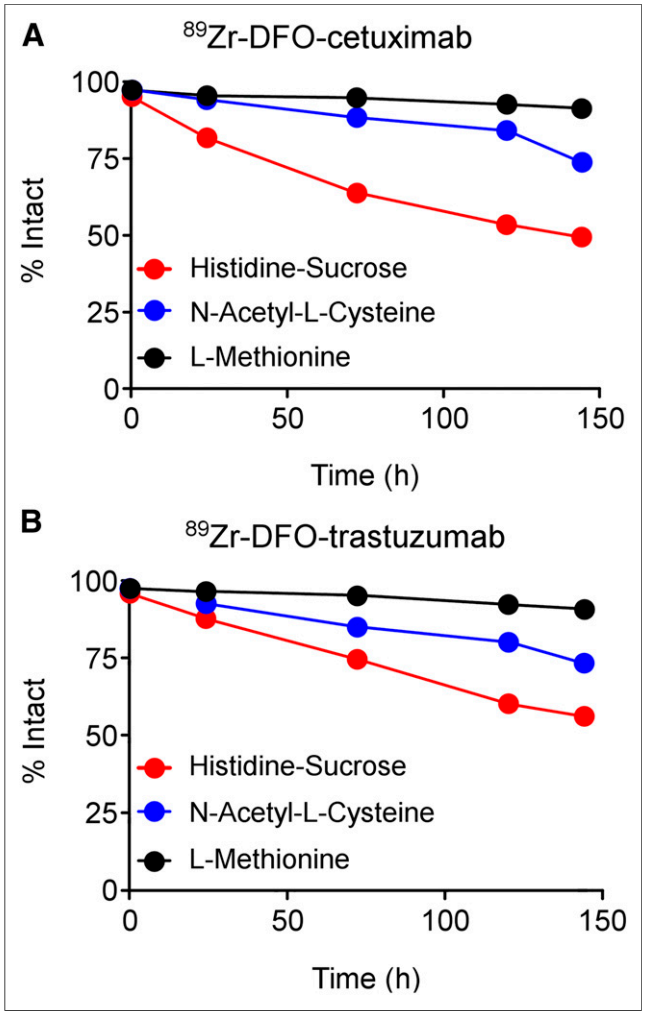


**FIGURE 1.** Summarized stability data obtained at 21°C. The 0.25 M NaOAc buffer containing 5 mg·mL$^{-1}$ L-MET was superior to other formulations at maintaining solution stability of $^{89}$Zr-DFO-cetuximab (A) and $^{89}$Zr-DFO-trastuzumab (B) during study. Percentage intact radiopharmaceutical was determined by subtracting total area under product peak from total area generated for all peaks in size-exclusion chromatogram and multiplying by factor of 100%. Each data point is average of 3 size-exclusion chromatography runs.

$^{89}$Zr-DFO-trastuzumab, prepared with $^{89}ZrCl_4$ or $^{89}Zr(ox)_2$, was evaluated using the Lindmo method (*13,14*). Data are presented in Supplemental Table 11 and Supplemental Figs. 9–11. $^{89}$Zr-DFO-trastuzumab prepared with $^{89}Zr(ox)_2$ demonstrated a $K_a$, $B_{max}$, and IR of $2.2 \times 10^8$ M$^{-1}$, $1.3 \times 10^8$, and 1.0, respectively. The respective values for $^{89}$Zr-DFO-trastuzumab prepared with $^{89}ZrCl_4$ were $2.4 \times 10^8$ M$^{-1}$, $1.3 \times 10^8$, and 0.91, respectively. No binding was observed in the HER2$^-$ 827 cell line.

Small-animal PET/CT imaging was performed. Representative images of 1 mouse that received $^{89}$Zr-DFO-trastuzumab prepared with $^{89}ZrCl_4$ are depicted in Figure 2, and maximum-intensity-projection images of all mice at 144 h are depicted in Supplemental Figure 12. Figure 3A depicts the change in tumor-to-muscle ratio during the study. HER2$^+$ tumor-to-muscle ratios were significantly greater than the HER2$^-$ tumor-to-muscle ratios at 144 h after injection (19.5 ± 3.3 vs. 8.1 ± 2.7, $P = 0.0003$). Average tumor-associated radioactivity in post-PET biodistribution studies is depicted in Figure 3B. Complete biodistribution data are provided in Supplemental Table 12. HER2$^+$ tumors retained more radioactivity than HER2$^-$ tumors at 144 h after injection (percentage injected dose/g, 29.5 ± 4.9 vs. 16.7 ± 6.1, $P = 0.0011$), but differences in tumor-associated radioactivity among mice receiving $^{89}$Zr-DFO-trastuzumab prepared with either $^{89}ZrCl_4$ or $^{89}Zr(ox)_2$ were not significant ($P = 0.30$). Additionally, the biodistribution of radioactivity in nontarget tissues between both cohorts was similar. For example, the amount of radioactivity in the bones of mice injected with $^{89}$Zr-DFO-trastuzumab prepared with $^{89}ZrCl_4$ was 8.3% ± 0.5%, whereas it was 7.8% ± 0.9% for mice receiving $^{89}$Zr-DFO-trastuzumab prepared with $^{89}Zr(ox)_2$.

## DISCUSSION

This work was undertaken to evaluate the use of $^{89}ZrCl_4$ in radiopharmaceutical synthesis and determine whether it provides any advantages as an $^{89}$Zr source. Initially, we prepared $^{89}ZrCl_4$ from $^{89}Zr(ox)_2$ using a previously published method (*7*), but buffering the 1 M HCl eluent containing $^{89}ZrCl_4$ allowed us to forego the cumbersome, inefficient, and dangerous drying step, which should make the use of $^{89}ZrCl_4$ more routine. Once $^{89}ZrCl_4$ was isolated, we compared $^{89}Zr(ox)_2$ versus $^{89}ZrCl_4$ in immuno-PET agent radiosynthesis by preparing $^{89}$Zr-DFO-trastuzumab and $^{89}$Zr-DFO-cetuximab using published procedures (*15–19*). We chose these mAbs since their radioactive analogs have been extensively characterized in the literature (*20–23*). Both radiopharmaceuticals

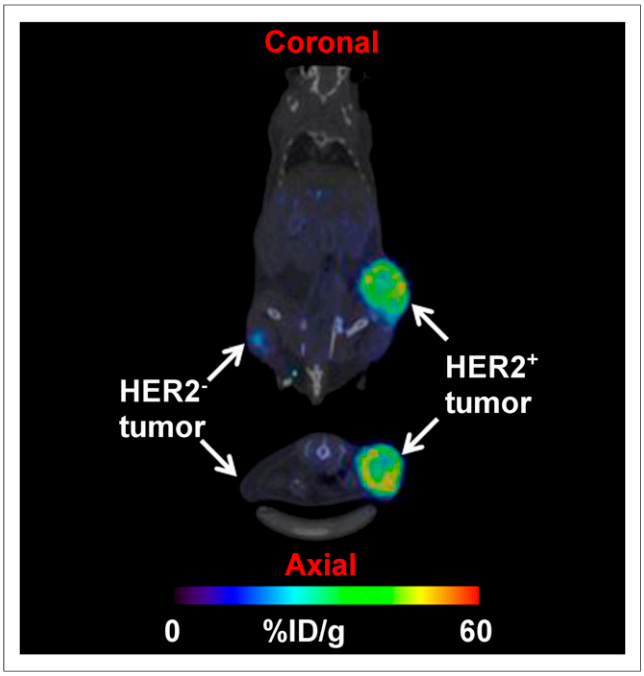


**FIGURE 2.** Representative PET/CT image of mouse bearing $HER2^+$ and $HER2^-$ tumors in contralateral flanks and imaged with $^{89}$Zr-DFO-trastuzumab. Coronal (top) and axial (bottom) sections of same mouse were imaged at 144 h. Images were taken from same anatomic location and equally scaled. More radioactivity was retained in $HER2^+$ tumor, suggesting that $^{89}$Zr-DFO-trastuzumab remains reactive toward antigen if injected immediately after preparation. Central necrotic core is observed within $HER2^+$ tumor.

were synthesized with increased specific activity, whereas reaction time was decreased to 15 min, since buffering with HEPES allowed us to skip the $Na_2CO_3$ neutralization step described in the literature (*15,16,18*). The solution reactivity of $^{89}Zr(ox)_2$ or $^{89}ZrCl_4$ may also account for our observations. Although $^{89}Zr(ox)_2$ is a highly stable organometallic complex in solution, $^{89}ZrCl_4$ most likely undergoes aquation (*5,24,25*). Without the presence of competing ligands, chelation occurs more rapidly (Supplemental Tables 2 and 3). A similar rationale was proposed to explain the formation of $^{89}$Zr-tetraazamacrocycles with $^{89}ZrCl_4$ (*8*).

Although $^{89}ZrCl_4$ seemed to improve $^{89}$Zr immuno-PET agent synthesis, the presence of aqueous $Cl^-$ ions has always been viewed as detrimental to radiopharmaceutical stability (*16,26*). Accordingly, we examined the in vitro stability of both radiopharmaceuticals after preparation with $^{89}ZrCl_4$. Initially, both radiopharmaceuticals were evaluated in 20 mM histidine/240 mM sucrose buffer since it preserves radiopharmaceutical integrity at 4°C or at 21°C better than does 0.9% saline (*26*). During the study's first 6 h, radiochemical purity remained above 95%. However radioactive high- and low-molecular-weight impurities formed by 24 h. We could not characterize these impurities, but size exclusion chromatography data and the literature suggest they are high-molecular-weight aggregates and low-molecular-weight species, such as smaller antibody fragments or the $^{89}$Zr-DFO complex generated by solution radiolysis (*26*). These observations spurred us to determine whether radiopharmaceutical purity could be maintained above 95% for an extended time, since it should yield better image quality. Moreover, maintaining stability is critical when many clinical sites rely on centralized radiopharmaceutical production facilities, often in different locations, to supply them with $^{89}$Zr immuno-PET agents for clinical use (*27*).

Previously, we demonstrated that NAC maintained long-term stability of radiopharmaceuticals (*11*). Moreover, a literature survey revealed that L-MET has also been used in radiopharmaceutical formulation where high energy particles and γ-ray photons are emitted during nuclear decay (*28*). Formulating the radiopharmaceuticals with NAC or L-MET allowed us to maintain radiopharmaceutical purity above 95% for at least 24 h. Both NAC and L-MET are sulfur-containing radical scavengers believed to suppress the formation of hydroxyl radical (·OH) and hypochlorous acid, which initiate several degradative mechanisms such as aggregation and fragmentation during radiopharmaceutical storage (*11,29*).

Based on Lindmo analysis, $^{89}$Zr-DFO-trastuzumab performed similarly regardless of preparative route, with $K_a$, IR, and $B_{max}$ consistent with the literature (*22,23*). Although tumor necrosis, which was independent of tumor size, led to variable amounts of radioactivity retained in tumors, the imaging data agreed with the in vitro data. $^{89}$Zr-DFO-trastuzumab underwent efficient clearance from nontarget tissues while accumulating in $HER2^+$ tumors, most likely by known receptor-mediated mechanisms. Radioactivity associated with $HER2^-$ tumors most likely results from perfusion effects, which would be consistent with

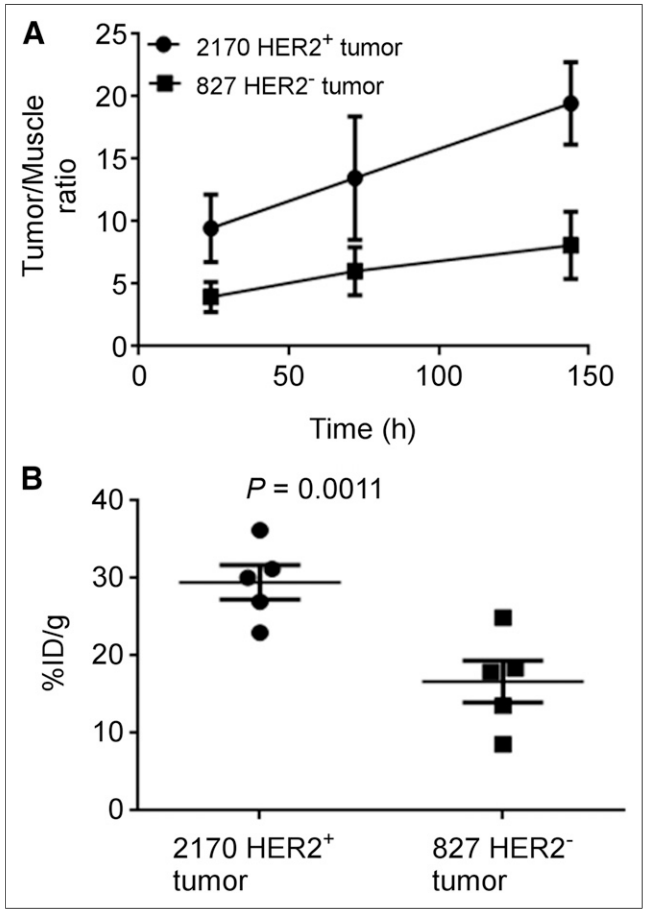


**FIGURE 3.** PET/CT data for mice injected with $^{89}$Zr-DFO-trastuzumab prepared with $^{89}ZrCl_4$. (A) Tumor-to-muscle ratios increase as $^{89}$Zr-DFO-trastuzumab undergoes clearance from nontarget tissues. (B) At 144 h, more radioactivity is retained in $HER2^+$ tumors, corroborating imaging data.

the literature (*22,23*). Bone marrow is considered a dose-limiting organ, and in $^{89}$Zr-radiopharmaceutical development, radioactivity levels in bone tissue are considered a surrogate indicator for radiopharmaceutical and $^{89}$Zr-DFO chelate stability (*5,30*). The amount of radioactivity associated with bone tissue was similar regardless of preparative route. This agrees with published literature and supports the idea that $^{89}ZrCl_4$ does not have an immediate detrimental effect on radiopharmaceutical stability or antigen reactivity in vivo (*20,22,23,26,31,32*).

Several limitations to these studies should be considered. Although the reaction of DFO-mAbs with $^{89}ZrCl_4$ required less time for completion, kinetic analyses, as described previously (*33*), were not performed. Stability studies were completed with $^{89}$Zr-DFO-trastuzumab and $^{89}$Zr-DFO-cetuximab, but in vitro and in vivo studies were completed only with $^{89}$Zr-DFO-trastuzumab, which was not formulated using NAC or L-MET. We used only trastuzumab for these studies since its stability under a variety of environmental conditions is less robust than cetuximab (*34*). Moreover, withholding NAC and L-MET enabled us to determine whether radiolysis, which is induced by ionizing radiation in the presence of aqueous chloride ions, had an immediate influence on radiopharmaceutical integrity and antigen reactivity and was prohibitive for radiopharmaceutical development. Our data suggests that there is a temporal window where $^{89}$Zr-radiopharmaceuticals prepared with $^{89}ZrCl_4$ retain sufficient purity to be used in cell and animal studies without the use of radical scavengers. However, adding them extends that temporal window by several days. Previously, we demonstrated that adding NAC to a solution of $^{89}$Zr-DFO-cetuximab did not affect its performance in vivo (*11*); a similar result would be expected here since NAC and L-MET have similar radical scavenging properties and improve stability over extended periods. Finally, our data suggest that $^{89}$Zr-DFO-mAbs prepared with $^{89}ZrCl_4$ or $^{89}Zr(ox)_2$ behave similarly in vitro and in vivo and are consistent with the literature (*22,23*), but our study cannot be directly compared with others because of differences in HER2 receptor expression among cell lines and tumor models.

Use of $^{89}ZrCl_4$ may offer several advantages, including lowering production costs and reducing radiation exposure. Additionally, it may facilitate the development of kit technology that can be used preclinically at sites that lack dedicated radiochemistry facilities, and thereby provide researchers greater access to immuno-PET studies. L-MET's superior protection of radiopharmaceutical integrity represents another noteworthy finding, since enhanced stability should yield better imaging results. Finally, using $^{89}ZrCl_4$ allows radiopharmaceuticals to be generated with significantly improved specific activity, which is an important outcome criterion in radiochemistry (*35–40*). Radiopharmaceuticals with high and nonvariable specific activity and formulated with common antioxidants should be more quickly approved by regulatory agencies responsible for ensuring the safety and efficacy of these agents in a clinical setting (*40*).

## CONCLUSION

These studies examined the use of $^{89}ZrCl_4$ in $^{89}$Zr immuno-PET agent synthesis. Using $^{89}ZrCl_4$, $^{89}$Zr-DFO-trastuzumab and $^{89}$Zr-DFO-cetuximab were synthesized with improved specific activity. Moreover, reactivity toward antigen was not significantly diminished. This work represents an initial scrutiny of $^{89}ZrCl_4$ in radiopharmaceutical development. Further studies involving additional antibodies, peptides, and nanoparticles are under way to assess the utility of this approach in the development of radiopharmaceuticals for precision medicine applications.

## DISCLOSURE

This research was supported by Wake Forest University Health Sciences, Wake Forest Innovations, and the North Carolina Biotechnology Center (2016-BIG-6524). This research is also supported by the Wake Forest Baptist Comprehensive Cancer Center Cell and Viral Vector Laboratory Shared Resource and by the Translational Imaging Program and the Tumor Tissue and Pathology Shared Resource, which are supported by the National Cancer Institute's Cancer Center Support Grant P30CA012197 (the content is solely the responsibility of the authors and does not necessarily represent the official views of the National Cancer Institute). Editorial assistance was provided by Karen Klein, MA, in the Wake Forest Clinical and Translational Science Institute, which is supported by UL1 TR001420 (principal investigator, Donald McClain). Thaddeus Wadas, Darpan Pandya, and Nikunj Bhatt have filed patents relating to this work. No other potential conflict of interest relevant to this article was reported.

## REFERENCES

1. Salgado R, Moore H, Martens JWM, et al. Steps forward for cancer precision medicine. *Nat Rev Drug Discov.* 2018;17:1–2.
2. Dugger SA, Platt A, Goldstein DB. Drug development in the era of precision medicine. *Nat Rev Drug Discov.* 2018;17:183–196.
3. Moradi-Kalbolandi S, Hosseinzade A, Salehi M, Merikhian P, Farahmand L. Monoclonal antibody-based therapeutics, targeting the epidermal growth factor receptor family: from Herceptin to Pan HER. *J Pharm Pharmacol.* 2018;70:841–854.
4. Jauw YW, Menke-van der Houven van Oordt CW, Hoekstra OS, et al. Immuno-positron emission tomography with zirconium-89-labeled monoclonal antibodies in oncology: what can we learn from initial clinical trials? *Front Pharmacol.* 2016;7:131.
5. Deri MA, Zeglis BM, Francesconi LC, Lewis JS. PET imaging with $^{89}$Zr: from radiochemistry to the clinic. *Nucl Med Biol.* 2013;40:3–14.
6. Abou DS, Ku T, Smith-Jones PM. In vivo biodistribution and accumulation of $^{89}$Zr in mice. *Nucl Med Biol.* 2011;38:675–681.
7. Holland JP, Sheh Y, Lewis JS. Standardized methods for the production of high specific-activity zirconium-89. *Nucl Med Biol.* 2009;36:729–739.
8. Pandya DN, Bhatt N, Yuan H, et al. Zirconium tetraazamacrocycle complexes display extraordinary stability and provide a new strategy for zirconium-89-based radiopharmaceutical development. *Chem Sci.* 2017;8:2309–2314.
9. Graves SA, Kutyreff C, Barrett KE, et al. Evaluation of a chloride-based $^{89}$Zr isolation strategy using a tributyl phosphate (TBP)-functionalized extraction resin. *Nucl Med Biol.* 2018;64-65:1–7.
10. Tang Y, Li S, Yang Y, et al. A simple and convenient method for production of $^{89}$Zr with high purity. *Appl Radiat Isot.* 2016;118:326–330.
11. Bhatt NB, Pandya DN, Rideout-Danner S, Gage HD, Marini FC, Wadas TJ. A comprehensively revised strategy that improves the specific activity and long-term stability of clinically relevant $^{89}$Zr-immuno-PET agents. *Dalton Trans.* 2018;47:13214–13221.
12. Burvenich IJ, Lee FT, Cartwright GA, et al. Molecular imaging of death receptor 5 occupancy and saturation kinetics in vivo by humanized monoclonal antibody CS-1008. *Clin Cancer Res.* 2013;19:5984–5993.
13. Lindmo T, Boven E, Cuttitta F, Fedorko J, Bunn PA Jr. Determination of the immunoreactive fraction of radiolabeled monoclonal antibodies by linear extrapolation to binding at infinite antigen excess. *J Immunol Methods.* 1984;72:77–89.
14. Ise N, Omi K, Nambara D, Higashiyama S, Goishi K. Overexpressed HER2 in NSCLC is a possible therapeutic target of EGFR inhibitors. *Anticancer Res.* 2011;31:4155–4161.
15. Perk LR, Vosjan MJ, Visser GW, et al. p-isothiocyanatobenzyl-desferrioxamine: a new bifunctional chelate for facile radiolabeling of monoclonal antibodies with zirconium-89 for immuno-PET imaging. *Eur J Nucl Med Mol Imaging.* 2010;37:250–259.

16. Vosjan MJ, Perk LR, Visser GW, et al. Conjugation and radiolabeling of monoclonal antibodies with zirconium-89 for PET imaging using the bifunctional chelate p-isothiocyanatobenzyl-desferrioxamine. *Nat Protoc.* 2010;5:739–743.
17. Vugts DJ, Visser GW, van Dongen GA. $^{89}$Zr-PET radiochemistry in the development and application of therapeutic monoclonal antibodies and other biologicals. *Curr Top Med Chem.* 2013;13:446–457.
18. Knight JC, Paisey SJ, Dabkowski AM, et al. Scaling-down antibody radiolabeling reactions with zirconium-89. *Dalton Trans.* 2016;45:6343–6347.
19. Cohen R, Vugts DJ, Stigter-van Walsum M, Visser GW, van Dongen GA. Inert coupling of IRDye800CW and zirconium-89 to monoclonal antibodies for single- or dual-mode fluorescence and PET imaging. *Nat Protoc.* 2013;8:1010–1018.
20. Aerts HJ, Dubois L, Perk L, et al. Disparity between in vivo EGFR expression and $^{89}$Zr-labeled cetuximab uptake assessed with PET. *J Nucl Med.* 2009;50:123–131.
21. Hoebers F, Aerts H, Van Loon J, Van Dongen G, Lambin R. Cetuximab zirconium, a new generation of functional imaging. *Eur J Cancer.* 2013;49(suppl):S80–S81.
22. Deri MA, Ponnala S, Kozlowski P, et al. p-SCN-Bn-HOPO: a superior bifunctional chelator for $^{89}$Zr immunoPET. *Bioconjug Chem.* 2015;26:2579–2591.
23. N Tinianow J, Pandya DN, Pailloux SL, et al. Evaluation of a 3-hydroxypyridin-2-one (2,3-HOPO) based macrocyclic chelator for $^{89}Zr^{4+}$ and its use for immuno-PET imaging of HER2 positive model of ovarian carcinoma in mice. *Theranostics.* 2016;6:511–521.
24. Singhal A, Toth LM, Lin JS, Affholter K. Zirconium(IV) tetramer/octamer hydrolysis equilibrium in aqueous hydrochloric acid solution. *J Am Chem Soc.* 1996; 118:11529–11534.
25. Hummel W, Anderegg G, Puigdomenech I, Rao L, Tochiyama O. *Chemical Thermodynamics of Compounds and Complexes of U, Np, Pu, Am, Tc, Se, Ni and Zr with Selected Organic Ligands.* Vol. 9. Amsterdam, The Netherlands: Elsevier Science; 2005:1–1130.
26. Vugts DJ, Klaver C, Sewing C, et al. Comparison of the octadentate bifunctional chelator DFO*-pPhe-NCS and the clinically used hexadentate bifunctional chelator DFO-pPhe-NCS for $^{89}$Zr-immuno-PET. *Eur J Nucl Med Mol Imaging.* 2017; 44:286–295.
27. Perk LR, Rispens SI. The future of immuno-PET in drug development. BV Cyclotron VU website. https://www.cyclotron.nl/library/resource/file/pdf/fsw20141015/cyclo_wp%231_web_141014.pdf. Accessed February 26, 2019.
28. Mueller D, Breeman WA, Klette I, et al. Radiolabeling of DOTA-like conjugated peptides with generator-produced $^{68}$Ga and using NaCl-based cationic elution method. *Nat Protoc.* 2016;11:1057–1066.
29. Hiller KO, Asmus KD. Formation and reduction reactions of alpha amino radicals derived from methionine and its derivatives in aqueous solutions. *J Phys Chem.* 1983;87:3682–3688.
30. Bhatt NB, Pandya DN, Wadas TJ. Recent advances in zirconium-89 chelator development. *Molecules.* 2018;23:638–662.
31. Price EW, Zeglis BM, Lewis JS, Adam MJ, Orvig C. H6phospa-trastuzumab: bifunctional methylenephosphonate-based chelator with $^{89}$Zr, $^{111}$In and $^{177}$Lu. *Dalton Trans.* 2014;43:119–131.
32. Williams SP. Tissue distribution studies of protein therapeutics using molecular probes: molecular imaging. *AAPS J.* 2012;14:389–399.
33. Kukis DL, DeNardo SJ, DeNardo GL, O'Donnell RT, Meares CF. Optimized conditions for chelation of yttrium-90-DOTA immunoconjugates. *J Nucl Med.* 1998;39:2105–2110.
34. Suárez I, Salmeron-Garcia A, Cabeza J, Capitan-Vallvey LF, Navas N. Development and use of specific ELISA methods for quantifying the biological activity of bevacizumab, cetuximab and trastuzumab in stability studies. *J Chromatogr B Analyt Technol Biomed Life Sci.* 2016;1032:155–164.
35. Lapi SE, Welch MJ. A historical perspective on the specific activity of radiopharmaceuticals: what have we learned in the 35 years of the ISRC? *Nucl Med Biol.* 2012;39:601–608.
36. Wessels BW, Rogus R. Absorbed dose calculations for radiolabeled tumor associated monoclonal-antibodies [abstract]. *J Nucl Med.* 1983;24(suppl):P95.
37. Wessels BW, Rogus RD. Radionuclide selection and model absorbed dose calculations for radiolabeled tumor associated antibodies. *Med Phys.* 1984;11: 638–645.
38. Mausner LF, Srivastava SC. Selection of radionuclides for radioimmunotherapy. *Med Phys.* 1993;20:503–509.
39. Bonardi ML, de Goeij JJM. How do we ascertain specific activities in no-carrier-added radionuclide preparations? *J Radioanal Nucl Chem.* 2005;263:87–92.
40. de Goeij JJM, Bonardi ML. How do we define the concepts specific activity, radioactive concentration, carrier, carrier-free and no-carrier-added? *J Radioanal Nucl Chem.* 2005;263:13–18.